Wear test of a magnetically shielded Hall thruster at 3000 seconds specific impulse

IEPC-2013-033

Presented at the 33rd International Electric Propulsion Conference,
The George Washington University • Washington, D.C. • USA
October 6 – 10, 2013

Richard R. Hofer,* Benjamin A. Jorns,† James E. Polk,‡ Ioannis G. Mikellides,§
and John Steven Snyder **
Jet Propulsion Laboratory, California Institute of Technology, Pasadena, CA 91109

Magnetic shielding is shown to reduce wall erosion by orders of magnitude at a specific impulse of 3000 s during a 113 h wear test of a Hall thruster operating at a power density 50% higher than nominal. Before the wear test, path finding experiments determined the throttling capabilities of the H6MS over 4.5-12 kW operation through assessments of the performance, stability, and thermal characteristics. Operation at 800 V, 9 kW was identified as the operating condition for the wear test. The H6MS was not designed to provide the high magnetic field intensities necessary at high specific impulse. As a result, physics-based simulations predicted that portions of the inner wall would be less well shielded than the outer wall due to the non-optimal shape of the magnetic field. These minor limitations are easily rectified in a thruster designed for operation at high specific impulse. Thrust, current oscillations, and plume profiles were essentially constant during the wear test. Post-test analysis revealed wear patterns consistent with the pre-test simulations, which provided additional confidence in the predictive capabilities of the numerical tools used. Magnetic shielding of the discharge chamber walls was demonstrated by the appearance of net carbon deposition on the channel walls and profilometry of the walls after the wear test. Our findings show that Hall thrusters can achieve magnetic shielding at high specific impulse and power density, paving the way for their use on deep-space missions seeking to exploit the extraordinary capabilities that magnetic shielding provides.

I. Introduction

MAGNETIC shielding in Hall thrusters is a technique that reduces discharge chamber erosion rates by orders of magnitude, effectively eliminating wall erosion as a failure mode. The physics of magnetic shielding were first described by JPL after Aerojet-Rocketdyne's BPT-4000 reached a zero-erosion state 5.6 kh in to a 10.4 kh wear test [1,2]. Subsequently, magnetic shielding was shown to reduce

* Senior Engineer, Electric Propulsion Group, 4800 Oak Grove Dr., MS 125-109, Pasadena, CA 91109, richard.r.hofer@jpl.nasa.gov. Associate Fellow AIAA.
† Associate Engineer, Electric Propulsion Group. Member AIAA.
‡ Principal Engineer, Propulsion, Thermal, and Materials Systems Group. Associate Fellow AIAA.
§ Principal Engineer, Electric Propulsion Group. Associate Fellow.
** Senior Engineer, Electric Propulsion Group. Senior Member AIAA.

erosion rates by three orders of magnitude in a series of simulations and experiments designed to validate the physics of magnetic shielding through modification of the H6 Hall thruster [3-6]. Through nearly 5 kh of wear testing in a zero-erosion configuration with the BPT-4000 and detailed simulations and experiments with the H6MS, the physics of magnetic shielding have been established for thrusters operating at 2000 s specific impulse and 4.5-6 kW discharge power. The extensibility of magnetic shielding to higher specific impulse [7], conducting wall materials [8], higher power [9], lower power [10], and higher power density are key questions now being addressed by NASA as the limits of magnetic shielding are explored. In the present investigation, we demonstrate the efficacy of magnetic shielding in reducing erosion rates by orders of magnitude in Hall thrusters operating at 3000 s specific impulse through a wear test of the H6MS operating at 9 kW. The demonstration extends the application of magnetic shielding by 50% in terms of specific impulse (2000 to 3000 s) and power density (6 to 9 kW on the same thruster).

Achieving long-lifetime at high specific impulse (~3000 s) has been a goal of NASA Hall thruster research since the turn of the century. Early work sought to understand the design attributes necessary to achieve high-efficiency operation [11-13]. Design methodologies were developed to regulate the electron current and achieve high-performance over wide throttling ranges [14-16]. Follow-on efforts began to address lifetime requirements through the introduction of a renewable channel wall [17,18]. This approach has been deprecated through the advent of magnetic shielding technology, which obviates the challenges of qualifying a high-temperature mechanism that must function flawlessly over tens of thousands of hours of thruster operation.

The extension of magnetic shielding to 3000 s specific impulse is an important milestone since reaching this level would extend the application of Hall thrusters to the vast majority of robotic and human missions that NASA is likely to pursue for the next several decades. In particular, NASA's Asteroid Initiative, which aims to robotically rendezvous with, capture, and return a 7-10 m asteroid to cis-lunar space for exploration by crew in the early 2020s, optimizes for a 3000 s specific impulse electric thruster that can process approximately 10,000 kg of xenon propellant for a 40 kW power system (250 kg/kW) [19,20]. Given that the BPT-4000 Hall thruster and NEXT ion thruster have demonstrated 100 kg/kW and 125 kg/kW, respectively, the lifetime requirements for the Asteroid Redirect Mission (ARM) are significant extensions to the demonstrated capabilities of electric thruster technology. The throughput capabilities of magnetically shielded Hall thrusters are expected to far exceed even these ambitious goals. Based on the wear rates observed in the H6MS wear tests, the throughput capability of magnetically shielded Hall thrusters exceeds 3000 kg/kW, a factor of twelve higher than required by ARM.

Such extraordinary capability is achieved by exploiting two fundamental properties of the Hall thruster discharge: 1) the isothermality of magnetic field lines and 2) the thermalized potential, $\phi_0 \approx \phi - T_{e0} \times \ln(n_e/n_{e0})$, which is constant along a magnetic field line if the electrons are also isothermal. Here, ϕ is the plasma potential, T_{e0} is the electron temperature, n_e is the plasma density, and n_{e0} is a reference plasma density usually chosen on channel centerline. Since the plasma density decreases towards the wall, the plasma potential must drop unless the electron temperature is negligibly small. Magnetic shielding seeks to achieve equipotentialization of the lines of force by shaping lines to extend deep in the channel where electrons are cold ($T_e < 5$ eV), thereby minimizing the potential drop due to the electron pressure term and sustaining potentials near the wall close to the discharge voltage. Further, since the sheath potential is a strong function of the electron temperature, the cold electrons reduce the sheath potential to just a few volts. With the plasma potential near the wall maintained at nearly the discharge voltage and the sheath voltage being small, the kinetic energy that ions gain through the potential drop in the plasma along surfaces can be reduced significantly and with it the wall erosion rate.

Increasing the specific impulse from 2000 to 3000 s increases the discharge voltage (V_d) from 300 to 800 V. Maximum electron temperatures increase with the discharge voltage, where in Hall thrusters it is generally found that $T_{e,max} \sim 0.1 * V_d$. The axial distribution of the electron temperature from the peak towards the anode is cooled, primarily through ionizing collisions, but relatively few measurements exist at high-voltage [21-25] showing if the population will cool sufficiently to marginalize the electron pressure term in the thermalized potential. Under such conditions, field lines must be shaped to extend very close to the anode in order to sample the lowest energy electrons in the discharge chamber. If this happens, the thruster would still be expected to be magnetically shielded.

In these experiments, we demonstrate with a thruster not optimized for high specific impulse that shielding can indeed be attained with 800 V discharges. We begin with a discussion of the experimental apparatus followed by a summary of the path finding experiments aimed at identifying the performance, stability, and thermal characteristics of a magnetically shielded Hall thruster operating at high power density and specific impulse. Predictions from physics-based modeling are provided that made specific predictions about the erosion rates. Results from the wear test conducted at 800 V, 9 kW are then presented in detail. We find that as expected magnetic shielding was attained over the 113 h wear test very well for the outer wall of the H6MS and to a lesser degree on the inner wall. The higher erosion rates on the inner wall are due to the limitations of the H6MS at these high voltages as the magnetic circuit was not designed for operation there. Our findings show that Hall thrusters can achieve magnetic shielding at high specific impulse and power density, paving the way for their use on ARM and other NASA missions seeking to exploit the extraordinary capabilities that magnetic shielding provides.

II. Experimental Apparatus

Photographs of the experimental configuration are shown in Figure 1. The thruster was mounted to a thrust stand in a large vacuum chamber. In front of the thruster, two different sets of translation stages were used to position probes in the near- and far-field plume. The near-field stages were not used for these experiments and were covered with graphite felt. The far-field stages consisted of a pair of linear stages for radial and axial translation as well as a rotary table so that the angle of a Faraday probe relative to the ion beam could be varied.

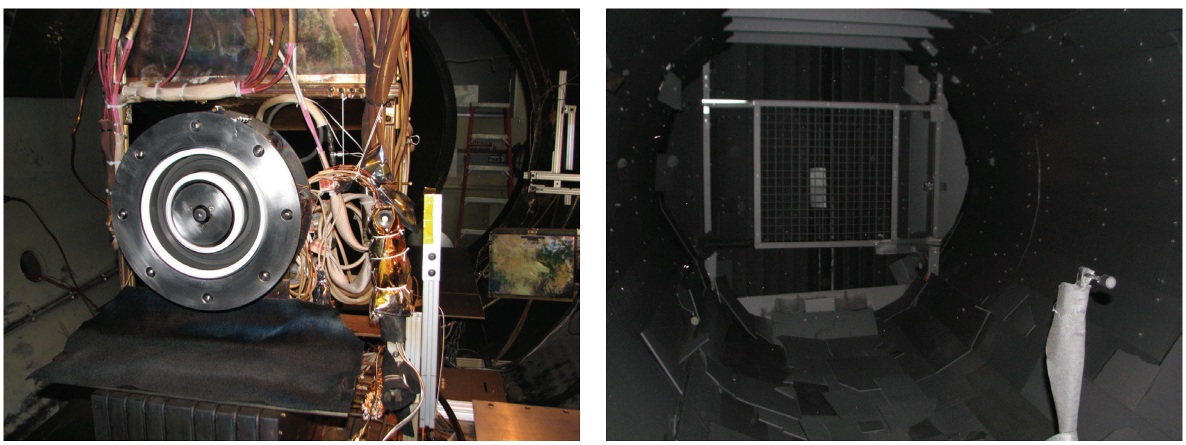

Figure 1 Photographs of the experimental configuration. Left: The H6MS installed on the thrust stand prior to starting the 113 h wear test. To the right of the thruster, the QCM and witness plate used for measuring the backsputter rate of carbon are visible. Right: View downstream of the thruster showing the graphite-lined vacuum chamber walls and the Faraday probe mounted to the far-field translation stages.

A. H6MS Hall Thruster

All experiments were conducted using the magnetically shielded (MS) version of the H6 Hall thruster, the H6MS. The original, unshielded (US) version of this laboratory thruster, the H6US, was a joint development between JPL, the University of Michigan, and the Air Force Research Laboratory [26]. High-performance is achieved through the use of a plasma lens magnetic field topography [14-16], a centrally-mounted lanthanum hexaboride (LaB_6) cathode [27,28], and a high-uniformity gas distributor/anode assembly [29]. The H6MS incorporates magnetic shielding that experiments show decreases wall erosion by three orders of magnitude relative to the US variant, effectively eliminating channel erosion as a failure mode [3-6]. The throttling range of the H6MS is approximately 0.6-12 kW discharge power, 1000-3000 s specific impulse, and 50-500 mN thrust. At the nominal 300 V, 6 kW condition, thrust, total specific impulse, and total efficiency of the H6MS are 384 mN, 2000 s, and 62.4%, respectively [3].

During the experiments, power and propellant were delivered to the H6 with commercially available power supplies and flow controllers. The plasma discharge was sustained by a pair of power supplies wired in parallel capable of up to 500 V, 40 A operation. The discharge filter consisted of an 80 μF capacitor in parallel with the discharge power supply outputs. Additional power supplies were used to power the magnet coils and the cathode heater and keeper. The cathode heater and keeper were used only during the thruster ignition sequence. Research-grade xenon (99.9995% pure) was supplied through stainless steel feed lines with 50 and 500 sccm mass flow controllers. The controllers were calibrated before the experiment and were digitally controlled with an accuracy of ±1% of the set point. The cathode flow rate was always set to 7% of the anode flow rate.

B. Vacuum facility

Experiments were performed in the Owens Chamber at JPL. The 3 m diameter by 10 m long, cryogenically-pumped vacuum chamber has been used previously to test gridded ion and Hall thrusters at power levels exceeding 20 kW. Pressure is monitored in the chamber using a pair of ionization gauges and a Residual Gas Analyzer (RGA). The RGA is connected to a gate valve attached to the chamber wall downstream of the thruster exit plane. This instrument is used to measure the partial pressures of the gases in the facility when the base pressure is reached. The first ionization gauge is calibrated for nitrogen and mounted to the chamber wall downstream of the thruster exit plane. This gauge is used to measure the base pressure of the facility. The second ionization gauge is calibrated for xenon and mounted below the thrust stand. This gauge is used to measure the operating pressure during thruster operation. For these experiments, the base pressure was typically $5x10^{-7}$ Torr or less. As indicated by the RGA, water vapor was the largest single background gas present, followed by nitrogen, oxygen, and mechanical pump oil. The nitrogen and oxygen partial pressures were as much as a factor of 100 less than the maximum recommended levels in Ref. [30,31] in order to avoid significant changes in insulator erosion. At a xenon flow rate of 13.41 mg/s, the operating pressure was $9.8x10^{-6}$ Torr, equivalent to a pumping speed of 176 kl/s at the standard temperature of 0 °C.

C. Thrust stand

Thrust measurements were acquired using a water-cooled, inverted-pendulum thrust stand with closed-loop inclination control and active damping [3,32,33]. Thermal drift and inclination of the thrust stand were accounted for during post-processing. Pressures of less than $2x10^{-5}$ Torr are sufficient to reliably obtain performance measurements without needing to correct for neutral gas ingestion [15,34]. This criterion was met in these experiments and no attempts to correct for neutral ingestion were made. Calibrations were performed by deploying a series of known weights ten times each [32]. When inclination and thermal drift were accounted for, the response of the thrust stand was repeatable and linear to the applied force. Analysis of thrust stand uncertainty indicated a range of ±1%. Given the uncertainty of the thrust, mass flow rate, current, and voltage, the uncertainty for specific impulse was calculated as ±1.4% and ±2.3% for efficiency.

D. Discharge current probe

A 20 MHz current probe and an 8-bit, 2 GHz oscilloscope were used to measure discharge current oscillations during steady-state thruster operation with an accuracy of ±3% [3,32]. The current probe was located on the anode side of the power input between the thruster and discharge filter described in section II.A. Oscillations were characterized by calculating the root-mean-square (RMS), peak-to-peak (P2P), and the power spectral density.

E. Thermal diagnostics

The temperature of various thruster components was measured using several different diagnostics. Type K thermocouples were mounted on the inner diameter of the inner front pole, the outer diameter of the outer front pole, the upstream end of the inner screen, and the downstream end of the outer screen. These signals were monitored continuously during the wear test using a data acquisition system that convert the thermoelectric potentials to temperature and correct for cold junction temperatures. The module calibrations were checked with a mV-level source. The uncertainty in the thermocouple reading is 2.2 °C [35].

The temperature of external thruster components was measured periodically throughout the test with a FLIR SC655 infrared imaging camera. This camera measures the thermal radiation emitted by a surface between wavelengths of 7.5 and 14 µm with a microbolometer detector and calculates a temperature based on inputs for the surface emittance and the transmission of any optical components. A 7° field-of-view IR lens was used to image the thruster through a ZnSe window with anti-reflective (AR) coatings mounted on the vacuum chamber 3 m from the thruster at an angle of 30° from the thruster centerline. Between measurements the window was covered with a shutter to protect the AR coatings from the ion beam. Based on the calibration data discussed in Ref. [35], the random uncertainty in the camera temperature measurements for a known emittance is less than ±2°C, but with an apparent systematic uncertainty of +3%. The uncertainty in measurements reported here is dominated by uncertainty in the assumed emittance for the components.

The emittance assumed in these measurements is based either on literature values or comparisons with *in situ* thermocouple data. Images of the downstream ends or exterior faces of the erosion rings were analyzed assuming an emittance of 0.87 based on thermocouple data obtained during thermal characterization tests [35]. Temperatures reported for the downstream face of the graphite cathode keeper assume an emittance of 0.77 [35]. Camera measurements on surfaces deep inside the discharge channel are assumed to be strongly influenced by reflection of infrared radiation from other hot surfaces in the cavity, and are not reported here. The uncertainty of the camera data based on potential errors in the emittances is ±12°C.

The average temperature of the magnet coils was inferred from the measured coil resistance and the temperature dependence of copper resistivity [35]. The resistance inferred from measured coil current and voltage is corrected for the resistance of the coil leads, which was measured separately. The estimated uncertainty of these temperatures is 3% below 500 K (227 °C) and 5% above 500 K, based on uncertainties in the electrical measurements and the uncertainty in the model for resistivity as a function of temperature.

F. Faraday probe

Shown in the right photograph of Figure 1, a Faraday probe used to measure ion current density was deployed in the far-field plume region. The probe consisted of a 1.91 cm diameter collection electrode enclosed within a 2.54 cm diameter guard ring. The guard ring and collector were separated by a 0.06-cm gap, were fabricated from graphite, and were biased −20 V below facility ground to repel electrons. The probe was positioned in the plume using a pair of linear translation stages and a rotary stage. The position of the probe is referenced to a radial-axial (r,z) coordinate system with the radial origin at the centerline of the thruster and the axial origin at the downstream exit plane of the discharge chamber. Axial and radial positions are normalized to the mean channel radius, R_m. The axial position of the probe was 13.2 R_m downstream of the thruster exit plane while the radial position was swept over ±7 R_m relative to thruster centerline. The probe face was aligned perpendicular to the thrust axis during the radial sweeps.

G. Erosion diagnostics

A Coordinate Measuring Machine (CMM) was used to measure the geometry of the insulator rings before and after wear testing. Wall profiles were obtained at four equally spaced locations around the circumference of a ring. Analysis of the various data sets taken during the experiments in Ref. [3] yielded an uncertainty of ±30 μm. Expressed as an erosion rate for a reference 10 h run time, the noise floor of the CMM is estimated to be ±1 μm/h.

A Quartz Crystal Microbalance (QCM) was used to measure the backsputter rate of carbon from the surfaces of the vacuum chamber subject to high-energy ion bombardment. The readout of the QCM was used in total deposition mode with the instrument parameters set for carbon deposition. A witness plate mounted next to the QCM (see Figure 1) made from boron nitride disks was used to validate the QCM settings by providing the average deposition rate over the entire wear test. The QCM was water-cooled and the temperature was monitored with a thermocouple. Radiation barriers and thermal insulation were used to thermally isolate the QCM from the thruster such that the temperature of the QCM was maintained to less than 1 °C. As shown in Figure 1, the QCM was axially positioned at the exit plane of the thruster discharge chamber and radially positioned within 3 cm of the thruster outer front pole. The uncertainty of the backsputter rate from the QCM measurements was estimated to be $\pm 0.5 \times 10^{-3}$ μm/h.

H. Gaussmeter

A Lakeshore Model 460 3-axis Gaussmeter was used to measure the applied magnetic field used during the wear test with coil currents corresponding to J_{ic}/J_{oc} = 5/5 A = 1. The Gaussmeter measurements were conducted with the discharge chamber removed from the thruster and the probe mounted on a two-axis translation system. The probe was aligned to within 0.05° of an *r-z* plane intersecting the thruster centerline. Positioning the probe at the discharge chamber exit plane and rotating the probe until the azimuthal field was nearly zero minimized the angular deviation of the probe's r-z sensors with respect to this plane. Data collection accounted for the finite separation of the radial and axial sensors by repositioning the probe for each (r,z) pair. The positional uncertainty did not exceed ±0.1 mm in any dimension. The uncertainty of the magnetic field was ±0.1 G.

III. Results

A. Path finding high-specific impulse experiments

Operation of the H6MS was studied over a series of path finding experiments demonstrating the discharge stability, performance, and thermal behavior over discharges voltages of 150-800 V and discharge powers of 4.5-12 kW. These studies were a critical step prior to the wear test since the operation of the H6MS had previously only been tested at 300 V, 6 kW [3-6]. Since the current studies were extensive, only a brief summary is provided here.

The experiments began with measurements of the discharge current-voltage characteristic as a function of magnetic field intensity. After establishing conditions for a stable discharge, thrust and discharge current oscillation measurements were obtained. The thermal behavior was assessed through observations of the discharge current stability with time and temperature measurements using the thermocouples and the IR camera.

Performance mappings demonstrated greater than 60% total efficiency over 300-800 V, 4.5-12 kW. Figure 2 shows the measured performance for various throttling profiles: constant 6 kW power, constant 15 A current, variable current as might be done for a deep-space mission, and 7-12 kW operation at 800 V. At 800 V, the increase in efficiency with power was likely dominated by mass utilization effects, which are well-known to strongly influence the efficiency of high-voltage Hall thrusters [14,15]. Total specific impulse exceeds 3000 s at 9 kW.

Dedicated thermal measurements were made during multi-hour firings at 9 and 10 kW power with the voltage at 800 V. At 9 kW, component temperatures were within the thermal limits expected of flight designs and it was decided to execute the subsequent wear test at this power level. At 10 kW and greater, higher temperatures were measured but this was at least in part due to magnetic circuit limitations discussed below.

The magnetic circuit of the H6MS was not designed to provide the high magnetic field intensities necessary for maximum efficiency at high-specific impulse [14]. This somewhat limits the efficiencies shown in Figure 2 as the coil currents increase with discharge voltage and the circuit begins to saturate. Maximum performance in the H6MS operating at 300 V, 6 kW corresponds to a current ratio of J_{ic}/J_{oc} = 4/3.31 = 1.21 for the inner and outer electromagnets [3]. Saturation of the outer magnetic circuit begins at J_{oc} = 4 A. If the coil current is maintained at the same ratio of 1.21, then the plasma lens field line topography will begin to be distorted when $J_{oc} > 4$ A, causing the plasma to contact the walls. Indeed, experiments at 800 V that purposely varied the coil current ratio by large margins demonstrated that wall heating could be induced by shifting the symmetry of the plasma lens from one wall to the next. The plasma lens shape can be corrected by increasing the coil current ratio towards unity, but the symmetry of the plasma lens across the discharge chamber centerline is not maintained due to saturation effects, which lowers efficiency. For operation at 800 V, 9 kW, it was determined that coil currents of J_{ic}/J_{oc} = 5/5 A = 1 minimized wall interactions and maximized efficiency. However, as shown in Figure 3 the grazing field lines at the channel exit were not symmetric. At the inner wall, the grazing line did not extend nearly as deep towards the anode as the outer wall grazing line. Since field lines are isothermal [5] and the electron temperature is decreasing towards the anode in this region of the discharge chamber, higher electron temperatures were expected for the inner wall grazing line, potentially increasing erosion rates. Indeed, this was observed in the wear test that followed (see section III.C), where it was found that the outer wall was very well shielded while the inner wall displayed two distinct regions where carbon deposition was decreased (i.e., higher erosion rates). Higher erosion rates on the inner wall relative to the outer wall were predicted prior to the wear test through physics-based simulation, discussed in section III.B.

The limitations of the H6MS magnetic circuit are in no way fundamental to Hall thruster design. Indeed, designs such as the NASA-173Mv2 have linear responses of the magnetic circuit at high field intensities [16]. Thrusters intended for 3000 s specific impulse at 12.5 kW power are now being designed by the GRC and JPL team that will alleviate the limitations of the H6MS magnetic circuit.

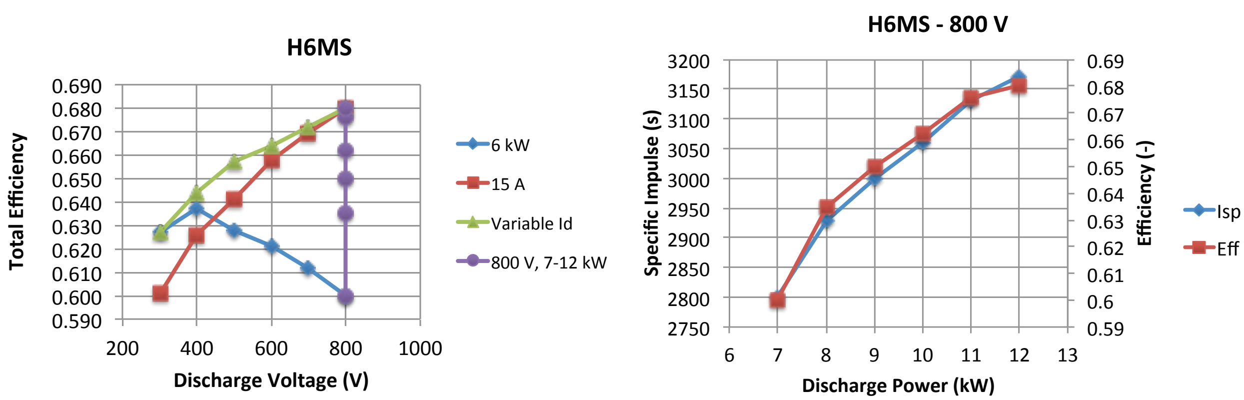

Figure 2 Performance of the H6MS over a range of operating conditions spanning 300-800 V and 4.5-12 kW. At 800 V, specific impulse greater than 3000 s is achieved at a discharge power of 9 kW.

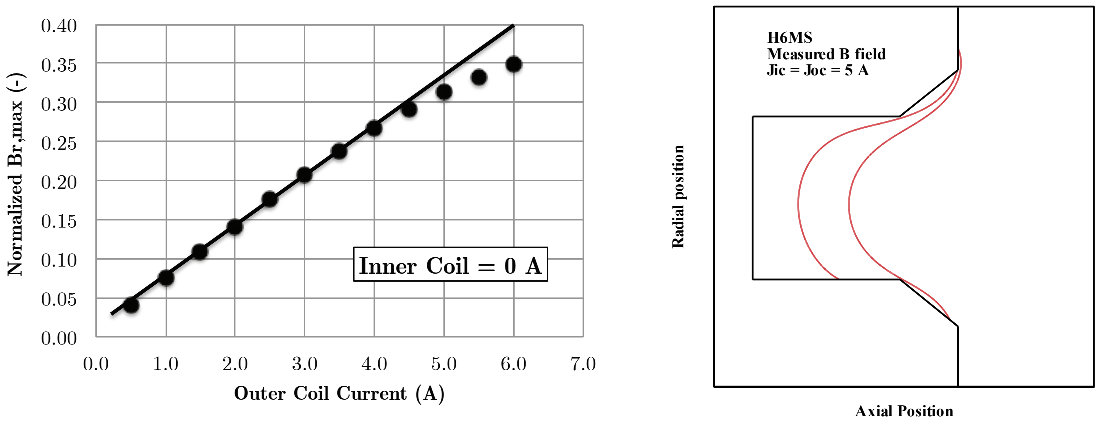

Figure 3 Left: Measured maximum radial magnetic field on discharge chamber centerline ($B_{r,max}$) in the H6MS as a function of outer coil current and the inner coil off. Above 4 A, the outer magnetic circuit begins to saturate. Right: Measured magnetic field lines in the H6MS with Jic/Joc = 5/5 A = 1. Magnetic circuit saturation at these coil currents distort the file line symmetry across the discharge chamber radius resulting in an outer wall grazing line that extends much deeper towards the anode than the inner wall grazing line. Higher erosion rates were therefore expected on the inner wall, a result predicted by physics-based simulation and observed in the wear test.

B. Modeling predictions at 3000 s specific impulse

Numerical simulations were performed with the Hall2De code [36] prior to the wear test to assess the effectiveness of magnetic shielding in the discharge voltage range of 300-700 V ($I_{sp} \approx$ 2000-2700 s) at 6 kW, and 800 V ($I_{sp} \approx$ 3000 s) at 9 kW. Detailed results of the simulations were reported in Ref. [7].

At 6 kW the magnetic field topology that we demonstrated magnetic shielding at 300 V [3-6] was retained for all other discharge voltages and it was found that magnetic shielding remained highly effective. Computed maximum erosion rates in the range of 300-700 V were found not to exceed 0.01 μm/h. Such rates are ~3 orders of magnitude less than those measured in the unshielded version of the same thruster at 300 V.

At 9 kW and 800 V saturation of the magnetic circuit did not permit us to attain the same magnetic shielding topology as that employed during 6 kW operation (see section III.A and Figure 3). Thus, it was not possible to extend the grazing field line along the inner wall as far upstream from the channel exit as at 6 kW, 300 V. It was expected that due to the higher electron temperature of the inner wall grazing line of force - caused by (1) its closer proximity to the downstream region of hot electrons and (2) the higher operating discharge voltage - the erosion rates could be higher at the two wall surfaces closest to this line than the rest of the inner wall. To the contrary, magnetic shielding of the outer wall at the 800 V, 9 kW condition was expected to be as effective as in the 300 V, 6 kW condition since the location of the grazing line along the outer wall was not significantly different.

Figure 4 summarizes the erosion rate predictions for the inner and outer wall from the 800 V, 9 kW simulations. Figure 4-left compares the total kinetic energy of ions bombarding the inner and outer walls. We found that the ion energy at the outer wall was below the minimum sputtering threshold of 25 V so no erosion was predicted here [7]. Near the downstream edge of the inner wall we found that the ion energy exceeded the 25 V threshold but was below 50 V, the maximum value we have determined the threshold of this material can attain. Assuming 25 V, Figure 4-right plots the computed erosion rate at the inner wall. We found that the maximum of ~0.15 μm/h is almost two orders of magnitude less than the value measured in the unshielded thruster at 300 V, 6 kW [7].

Since the inner wall grazing line did not extend as deep towards the anode as the outer wall grazing line, an additional analysis was conducted to examine the sensitivity of the computed erosion rates at the inner wall grazing line. The computed electron temperature contours near the inner wall from the 800 V, 9 kW simulations are shown in Figure 5-left. Also shown are the grazing field line along the inner wall and a line that passes by the downstream edge of the chamfered wall. Electron temperature at points A and B was computed to be 4.3 eV. At this value we found the total energy of ions at point B to be below the minimum sputtering yield threshold of 25 V and therefore no erosion was predicted by the simulation as shown in Figure 5-right. However, because the sputtering yield at these low energies is extremely sensitive to changes in the ion energy, a sensitivity analysis on the dependence of erosion rate on electron temperature revealed that a change of only ~1.5 eV would force the erosion rate at this point to exceed the carbon deposition rate of 0.0025 μm/h that was measured during the wear test. We found the plasma potential along the inner wall to be held very near to the discharge voltage so the increase in the erosion rate was caused largely by changes in the energy gained by ions in the sheath. We found that at point B an increase of 1.5 eV yielded an increase of ~6 V in the sheath potential, which is sufficient to raise the total ion energy above the assumed sputtering threshold. It is noted that changes of 1.5 eV (~0.1 % of the maximum electron temperature) are well within both the simulation and experimental uncertainties. Thus, it was predicted prior to the wear test that the erosion rates on the inner wall would be higher near the intersection points of the grazing field line.

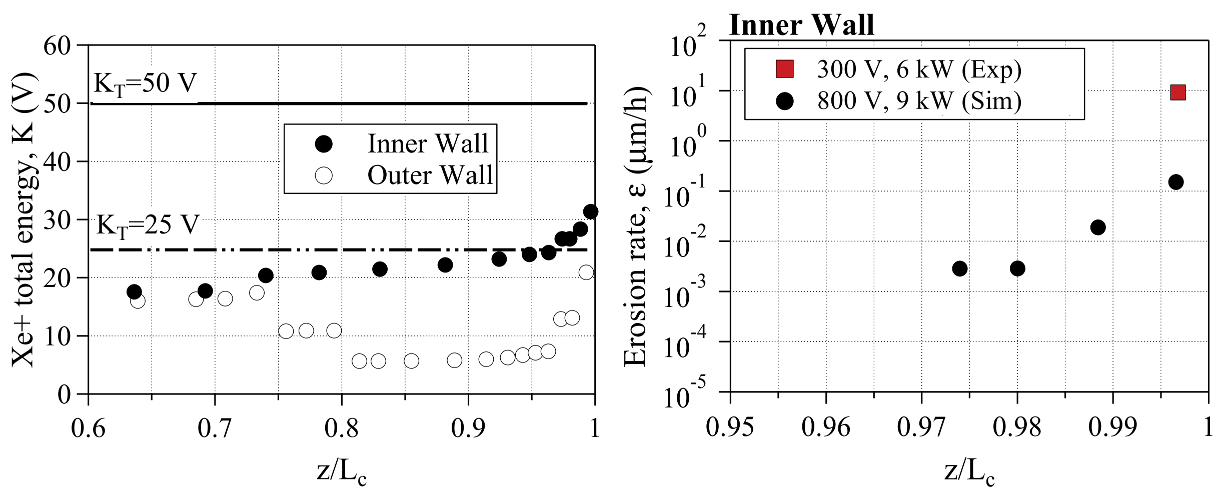

Figure 4 Left: Computed energy of singly-charged ions striking the channel walls from the 800 V, 9 kW simulations. The two horizontal lines at 25 and 50 V bound the range of possible sputtering yield thresholds for the BN walls. Right: Computed erosion rate of BN at the inner wall. Also shown is the maximum erosion rate measured during unshielded operation of the H6 at 300 V, 6 kW.

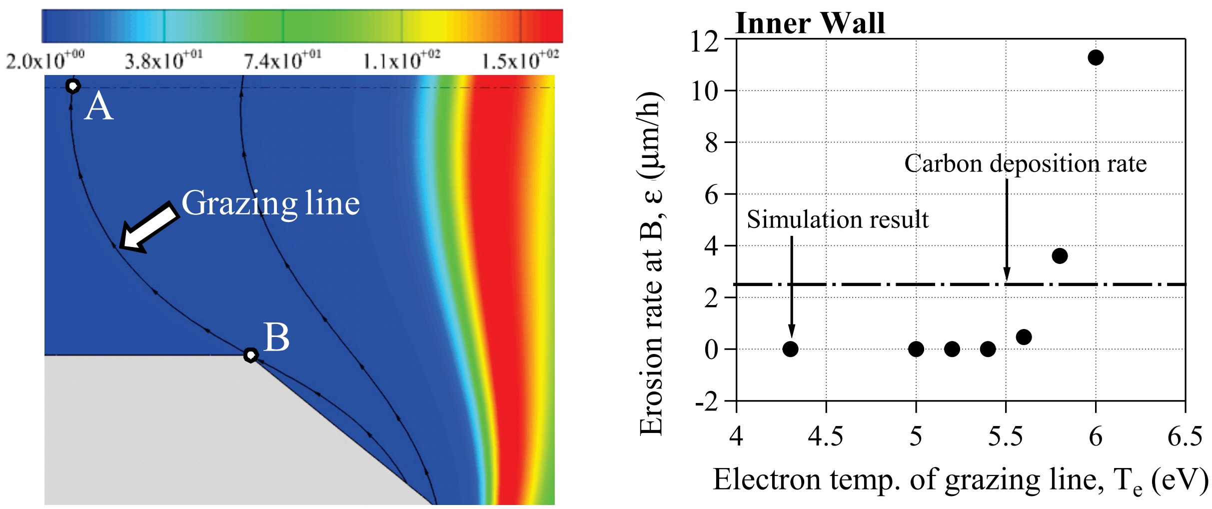

Figure 5 Left: Computed electron temperature contours (in units of eV) near the inner wall at 800 V, 9 kW. Also shown is the grazing field line (passing through points A and B) and a field line that just grazes the downstream edge of the wall. Electron temperature along the upstream and downstream lines is 4.3 eV and 5.9 eV, respectively. Right: Computed erosion rate at point B as a function of electron temperature. Only ~1.5 eV higher electron temperature along the A-B grazing line would increase the erosion rate to greater than the measured (0.0025 μm/h) carbon deposition rate.

C. 3000 s specific impulse wear test

Results from the performance, thermal, and stability experiments combined with the erosion simulations indicated that a wear test of the thruster at 800 V, 9 kW would be successful in demonstrating magnetic shielding at 3000 s specific impulse. Previous magnetic shielding investigations executed under controlled conditions were limited to 19 h, so it was decided to extend the 3000 s specific impulse wear test to greater than 100 h.

The primary objective of the wear test was to demonstrate magnetic shielding of the discharge chamber walls. Depicted in Figure 6, the discharge chamber of the thruster is designed with replaceable boron nitride rings. These rings have axial lengths that overlap the acceleration zone, such that new parts can be fabricated to accommodate design changes or wall diagnostics. New rings were fabricated prior to the wear testing phase of these experiments. The anode and the remaining portion of the BN discharge chamber walls were not cleaned prior to the test, which were well coated with a carbon film from previous testing. Although not controlled, the wear test was also conducted to examine how the front pole pieces and the cathode keeper would fare during longer run times. The iron pole pieces were sanded clean prior to the wear test. The graphite keeper, which is the original cathode built for the H6US, was not cleaned prior to the wear test.

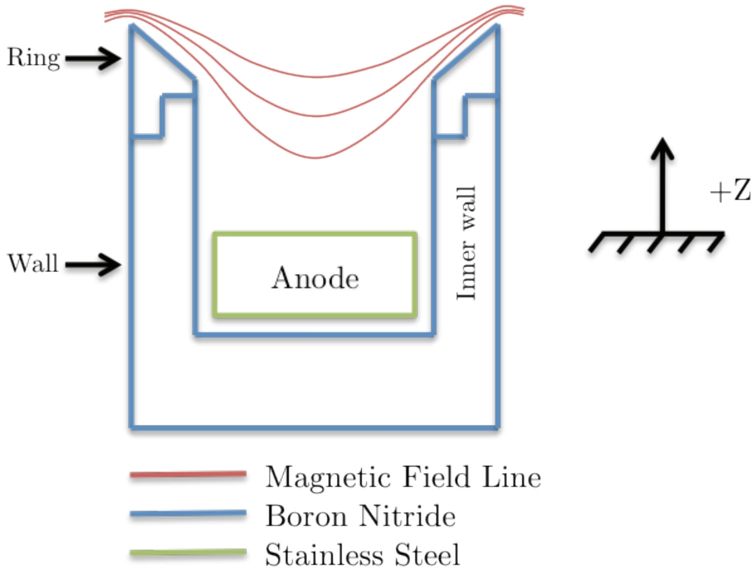

Figure 6 Schematic illustrating the segmented discharge chamber geometry and notional magnetic field of the H6MS. New erosion rings were machined for the wear test. Not to scale.

The wear test began February 14, 2013 and was concluded 12 days later. Since the rings were new, extra care was taken with bringing the thruster to 800 V by allowing sufficient time for the rings to outgas. No loss of discharge was sustained during this period. In fact, the discharge was maintained continuously over the entire wear test except for the following reasons: 1) loss of power at JPL that also led to a loss of vacuum, 2) data system communication errors that caused automated shutdowns, 3) and shutdowns for thrust stand zeros.

Chamber pressure measured by the xenon calibrated ionization gauge below the thrust stand is shown in Figure 7. Outgassing from the discharge chamber walls stopped after two hours of operation. The graphite-lined chamber walls continued to outgas until t ~ 45 h. This long period may have been influenced by the thruster operating condition (800 V, 9 kW) which was substantially higher than how the thruster is typically operated (300 V, 6 kW) in the chamber and may have caused the beam to impinge on different parts of the chamber than normal, inducing higher outgassing rates.

Table 2 summarizes the top-level results from the wear test. The operating condition of 800 V, 11.25 A was maintained 98.3% of the time during 114.6 h of operation. The equivalent run time at 9 kW was computed by dividing the total expended energy (1013.63 kW-h) by the total run time, resulting in 112.63 h of operation. During this time, 5.48 kg of xenon were processed. The longest continuous firing time that the thruster was allowed to operate between thrust stand zeros was 47 h.

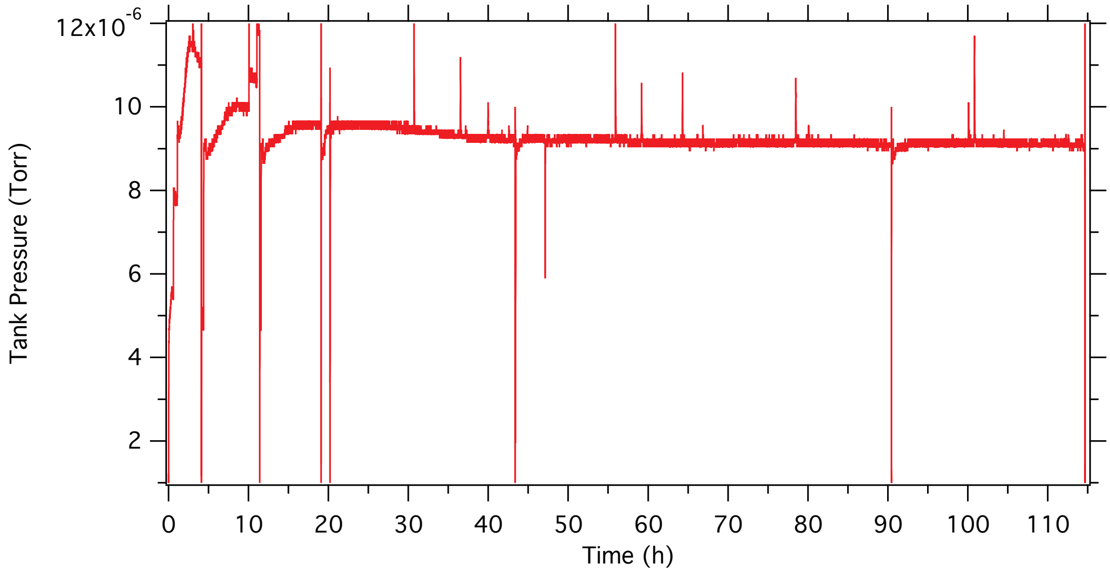

Figure 7 Tank pressure measured by the xenon calibrated ionization gauged mounted below the thrust stand. Outgassing from the thruster decreased after the first two hours while the chamber walls showed signs of outgassing until t ~ 45 h.

Table 1 Summary of operation during the 113 h wear test.

	P_d = 9 kW I_{sp} = 3000 s
Anode propellant throughput (kg)	5.12
Cathode propellant throughput (kg)	0.36
Total expended energy (kW-h)	1013.63
Total thruster operating time (h)	114.6
Equivalent run time at discharge power (h)	112.63
Longest continuous firing time (h)	47

Figure 8 show the discharge voltage and current over the entire run wear test. Except during startup periods, the discharge voltage was set to 800 V. The mass flow rate to the thruster was manually controlled by adjusting the flow until the discharge current reached ~11.25 A. After the outgassing phase in the first few hours, the discharge current drift was very low, typically ±0.05 A (±0.4%) over several hours of operation when the flow was held constant. For example, Figure 8 highlights a 17 h window where the flow was held constant and the average discharge current was 11.279 +0.049/-0.036 A.

Figure 9 shows the cathode floating potential with respect to facility ground during the wear test. The cathode potential varied as much as 4 V during the first 20 h of the wear test and then began to settle in towards -12 V. After the first 20 h of the wear test, the cathode potential variation over time was typically less than a volt. Figure 9 highlights a 40 h window over which the cathode potential averaged -12.1 ±0.8 V. Voltage variations of this magnitude are typical for this thruster and consistent with other Hall thruster wear tests. However, voltage hash in the cathode potential was noted to begin around t = 40 h and persist until the end. The cathode did not exhibit any obvious signs of damage after the experiment and has continued to be used without any issues for about 200 h more.

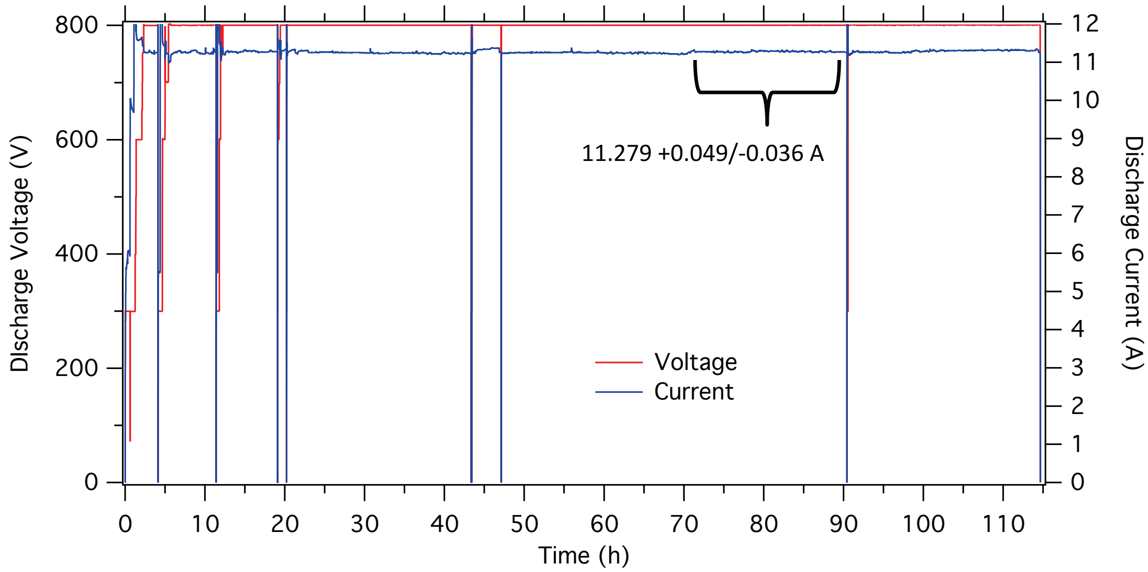

Figure 8 Discharge voltage and current during the 3000 s specific impulse, 9 kW discharge power wear test. Mass flow rate was held constant over many hours while the discharge current ran open loop. After the initial outgassing phase, discharge current drifts were exceptionally small. Over one 17 h window, the discharge current variation was less than 0.05 A (0.4%).

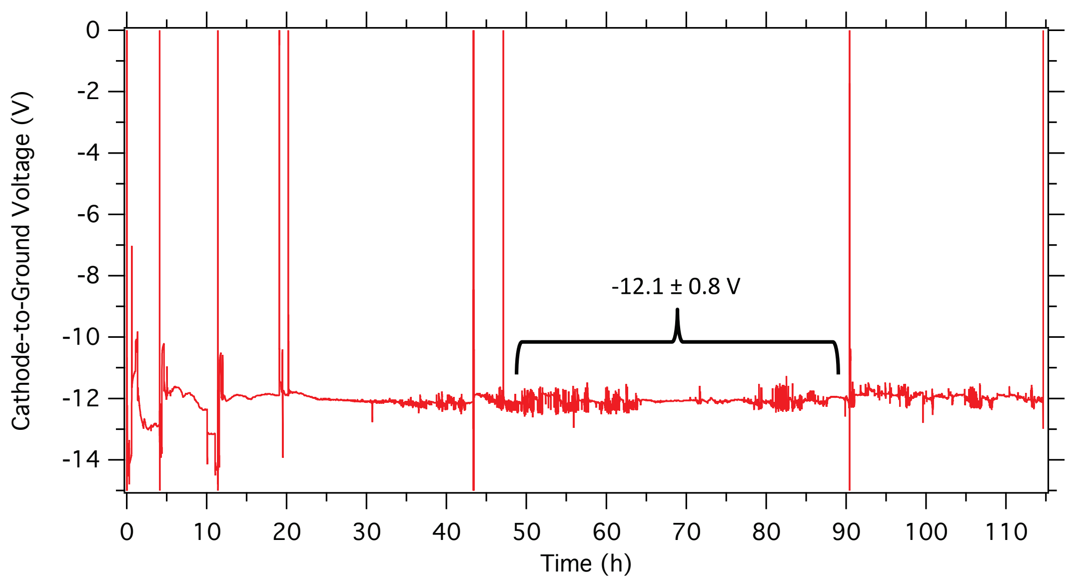

Figure 9 Cathode potential with respect to facility ground during the wear test. After t > 20 h of operation, the cathode potential variation was typically less than one volt.

The thruster thermal behavior during the wear test is shown in Figure 10 and Figure 11. Figure 10 shows the thermocouple (lines) and camera data (points). The transients represent thruster starts, and the remainder of the data indicate that the steady-state front pole, screen, and ring temperatures were very stable over the test, although the ring data indicate azimuthal variations of as much as 90 °C. The outer front pole temperature dropped steadily during the test, with a total change of 20 °C.

The magnetic coil temperatures inferred from resistance measurements are plotted in Figure 11. The outer coil temperature also dropped steadily (a total of 9 °C) during the test, probably as a result of the decreasing front pole temperature. As shown in Figure 12, varying the emittance in order to match the camera data to the thermocouple data for the inner and outer front pole yielded results suggesting that the outer pole emittance changed by about 50% during the test while the inner pole emittance was relatively constant. The increase in effective emittance for the outer pole was likely caused by backsputtered carbon deposition on the iron. The higher emittance is probably why the temperature of the outer pole (and the outer electromagnets, which are attached to that pole) decreased over time.

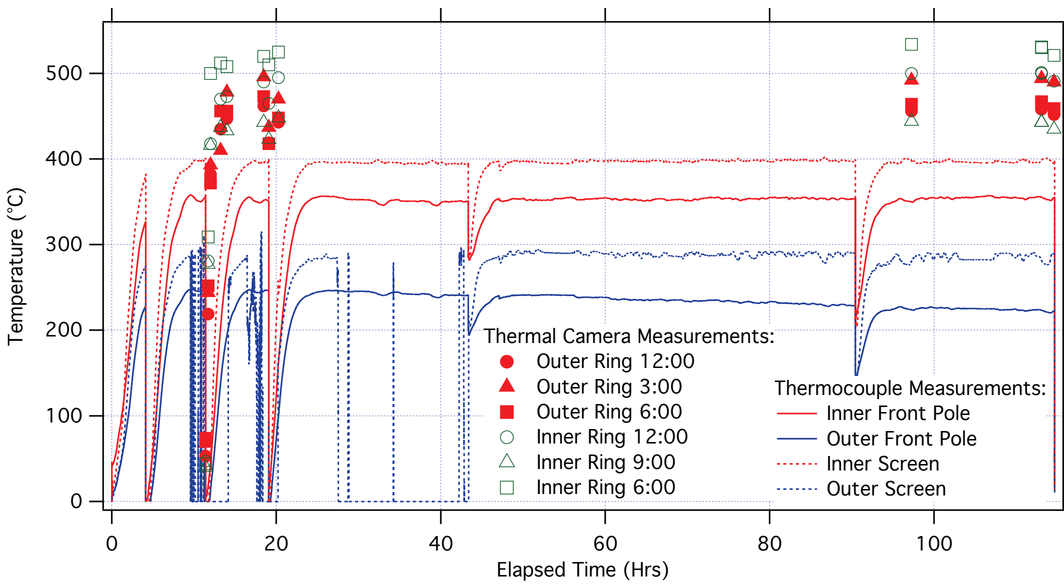

Figure 10 Temperatures measured with the thermocouples and thermal camera during the wear test.

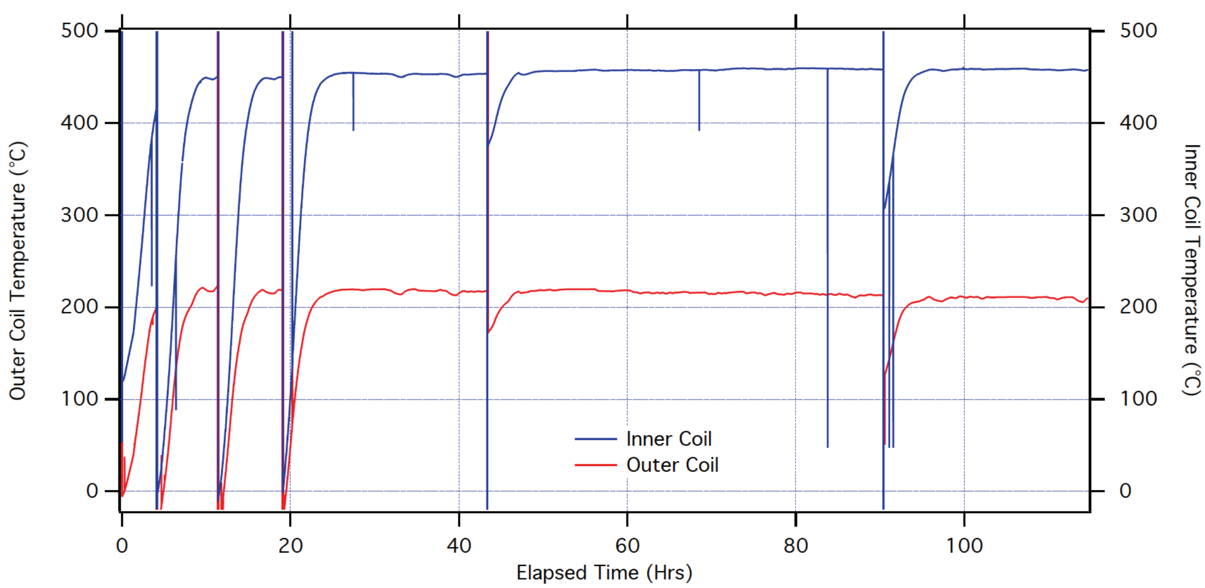

Figure 11 Magnet coil temperatures calculated from resistance measurements during the wear test.

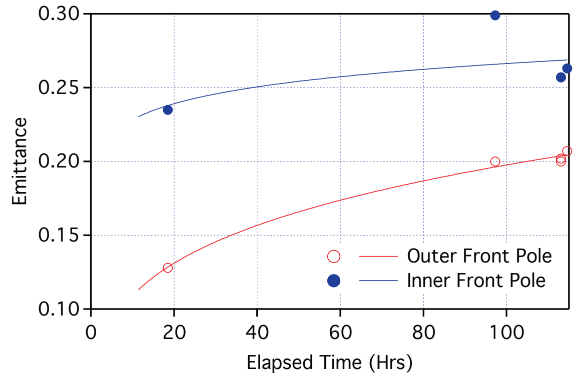

Figure 12 Front pole emittance during the wear test estimated by matching thermal camera measurements to thermocouple data. The large increase in the outer front pole emittance likely resulted from backsputtered carbon deposition from the vacuum chamber walls.

Performance measured during the wear test is shown in Figure 10 and tabulated in Table 2. The first thrust stand measurement occurred at t = 4 h, which was the highest thrust measured during the wear test. Outgassing from the thruster had subsided by t = 2 h, but the vacuum chamber was still outgassing (see Figure 7). Subsequent thrust measurements showed a ~1.2% thrust decrease after which thrust was constant over 100 h of operation. These small changes in thrust are possibly related to the formation of a carbon layer on the erosion rings, which could make them perform similar to the graphite-walled version of the H6MS [8]. Performance was essentially constant over a 100 h window, which was expected since the wall geometry was not changing during this time since the walls were not eroding as they would in unshielded Hall thrusters. This is an important benefit of magnetically shielded Hall thrusters since constant performance simplifies mission planning.

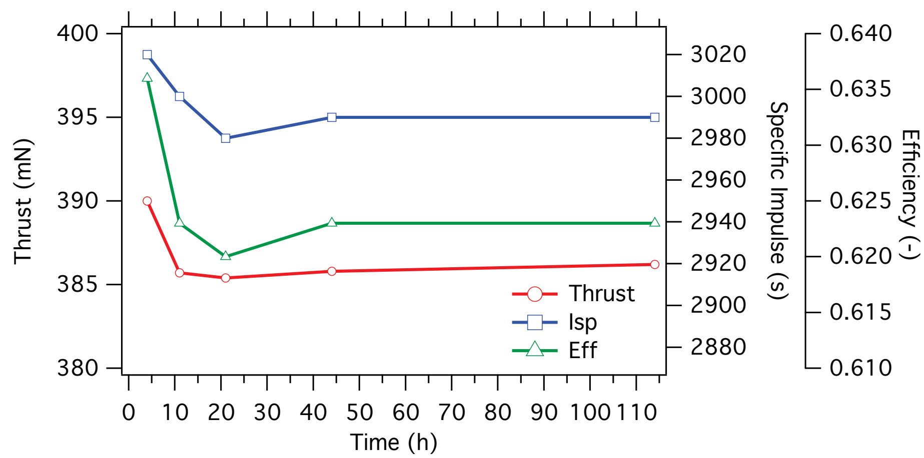

Figure 13 Performance over the wear test. Thrust was constant over 100 h of operation.

Table 2 Performance over the wear test.

Time (h)	T (mN)	Isp (s)	Efficiency (-)
4	390	3020	0.636
11	385.7	3000	0.623
21	385.4	2980	0.62
44	385.8	2990	0.623
114	386.2	2990	0.623

The power spectral density (PSD) of the discharge current oscillations at the beginning and end of the wear test is shown in Figure 14. PSD's of the intermediate times are omitted for clarity. Table 3 compares the RMS, P2P, and primary frequency from the spectra in Figure 14. The spectra show that the character of the PSD was essentially unchanged over the wear test. The RMS values differ by just 1% and the primary frequency of the oscillations is identical. Jorns has shown that the 68 kHz mode is related to cathode oscillations [37]. Harmonics of the cathode oscillations are also present above the primary mode at 68 kHz. The breathing mode frequency is 31-34 kHz, but is almost two orders of magnitude lower than the cathode oscillations. Broad-band noise at 3-6 MHz is also present, but is 5-7 orders of magnitude lower than the breathing mode and cathode oscillations.

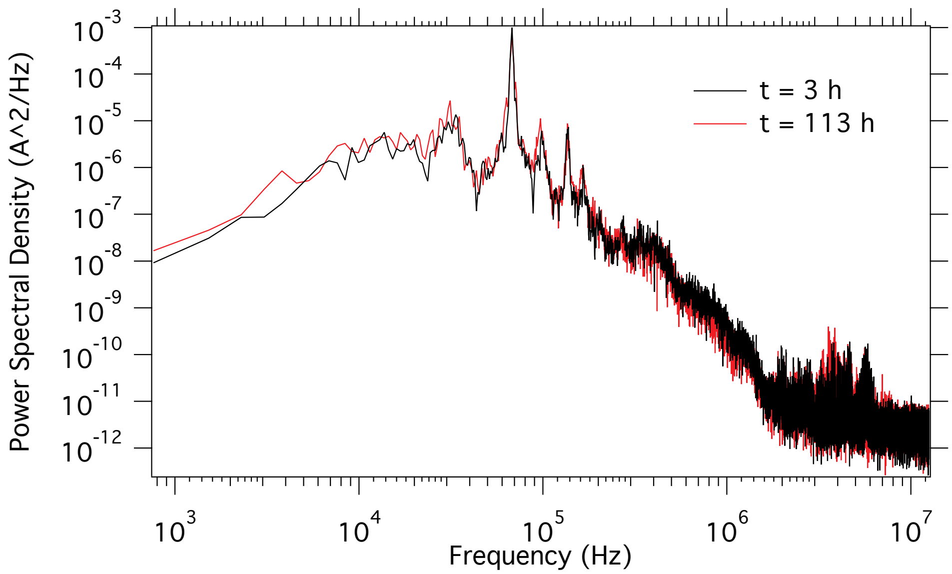

Figure 14 Power spectral density of the discharge current oscillations during the wear test.

Table 3 Discharge current properties during the wear test.

Time (h)	RMS (% mean)	P2P (% mean)	Frequency (kHz)
3	13	56	68
113	12	61	68

Ion current density profiles measured in the far-field plume are shown in Figure 15. The profiles are essentially unchanged during the entire wear test, which was expected since the wall geometry was not changing. The plume structure exhibits the "double-peak" structure typical of well-focused Hall thruster beams [15].

Figure 16 shows photographs of the H6MS before and after the 113 h wear test. After the wear test, the pole pieces and erosion rings all showed signs of net carbon deposition indicating that erosion rates from ion bombardment were extremely low. The carbon backsputter rate calculated from the QCM and witness plate data was 0.0025 μm/h.

Figure 17-left is a photograph of the inner front pole and cathode keeper after the wear test. Carbon deposition covered most of the inner front pole with the exception of a lighter colored film near the outer radius. The cathode keeper showed evidence of a ring of discoloration similar to the erosion that developed in the NSTAR discharge cathode [38]. The ring later disappeared when the thruster was tested at different operating conditions after the wear test. Machining marks from when the cathode was

fabricated (more than 1,000 h of thruster operation ago) are still visible. Although high-energy ion bombardment of the cathode keeper may be occurring in this region, it is not yet clear if erosion in this region is significant. Figure 17-right is a photograph of the outer front pole after the wear test. Various bands of carbon deposition were visible. The light colored band in the photograph was easily removed with a razor blade. Raman spectroscopy revealed that the material was predominately carbonaceous (micro-graphitic carbon).

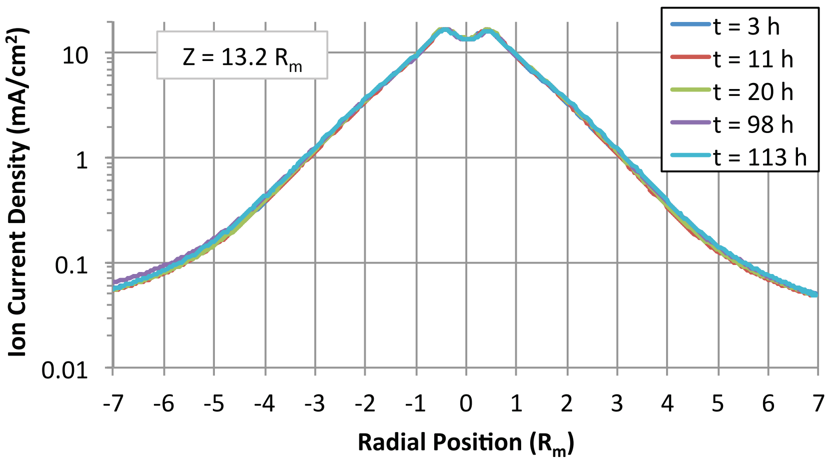

Figure 15 Ion current density profiles during the wear test were essentially constant. This was expected since the wall geometry was not changing.

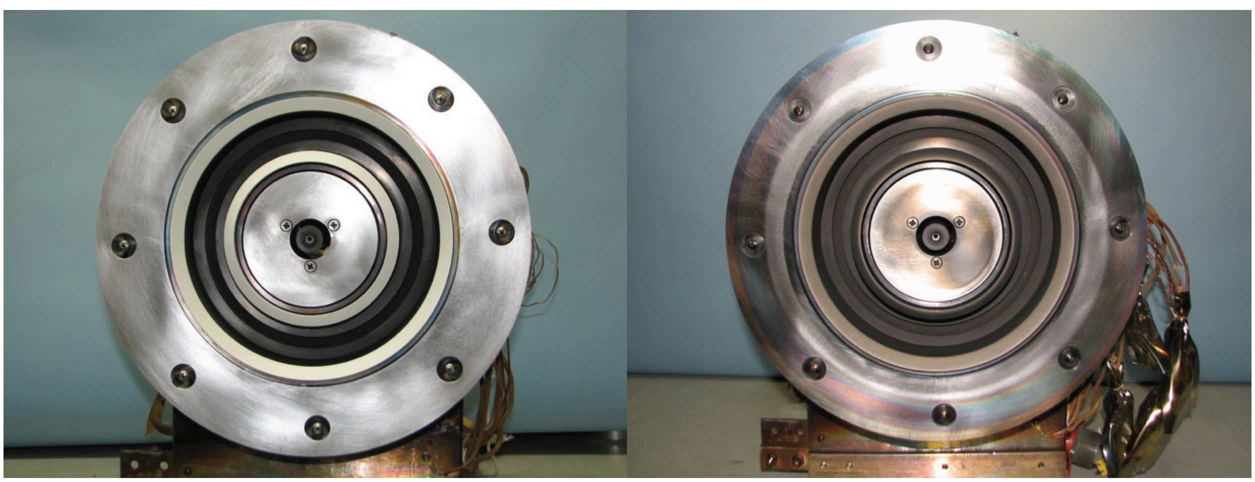

Figure 16 Photograph of the H6MS before (left) and after (right) the wear test. Before the wear test, the pole pieces were sanded clean and the erosion rings were replaced with new parts. After the wear test, the pole pieces and erosion rings were coated, to various degrees, with backsputtered carbon. The carbon backsputter rate was measured to be 0.0025 μm/h.

The carbon deposition on both rings was consistent with predictions made before the test (see Section III.A and B). Figure 18 compares the measured grazing field line (left) with a photograph of the deposition pattern observed on the inner wall erosion ring after the wear test (right). Arrows in Figure 18 point to regions on the inner wall where the deposition is much lighter than the rest of the ring. These two locations correspond to where the grazing field line was measured to intersect the wall. Since this field line does not extend deep in to the channel the electron distribution has not completely cooled, leading to higher erosion rates at the walls. In contrast, Figure 19 is a photograph of the outer wall erosion ring showing a uniform coating of carbon over the entire ring. Circumferential machining marks from fabrication were still visible on the surface of the outer ring. The improved shielding of the outer ring was expected since the outer wall grazing line extended deep in to the channel where the electron temperature is low.

Figure 17 Left: Photograph of the inner front pole and cathode keeper after the wear test. Carbon deposition was evident over most of the inner front pole. A ring of discoloration was evident on the cathode keeper, similar to erosion patterns observed with the NSTAR ion thruster discharge cathode assembly. However, machining marks were still visible after the wear test, so it is not clear if significant erosion was occurring here. Right: Photograph of the outer front pole after the wear test. Various bands of backsputtered carbon were evident on the outer front pole. The light colored region was easily removed with a razor blade after the wear test.

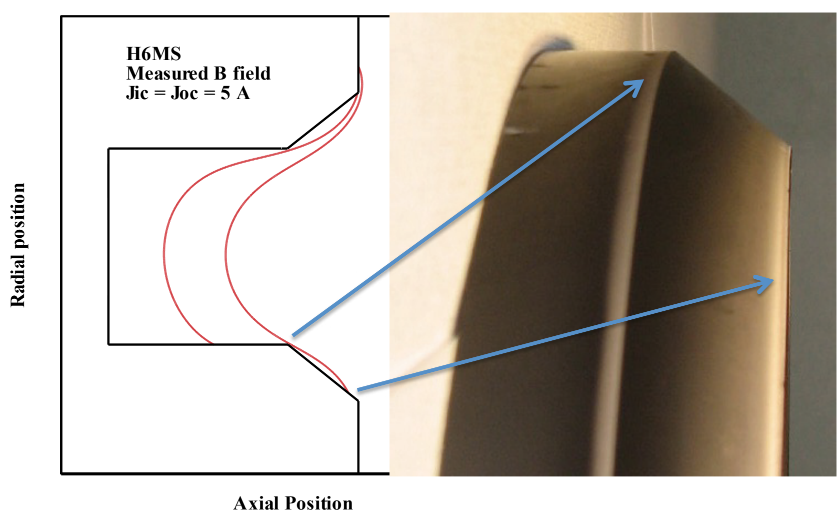

Figure 18 Measured grazing field lines in the H6MS (left) and the inner erosion ring after the wear test (right). Lighter-colored regions of reduced deposition on the inner ring match the inner wall grazing line, as expected. Since the inner grazing line does not extend as deep towards the anode as the outer grazing line, higher electron temperatures persist, increasing the local erosion rates.

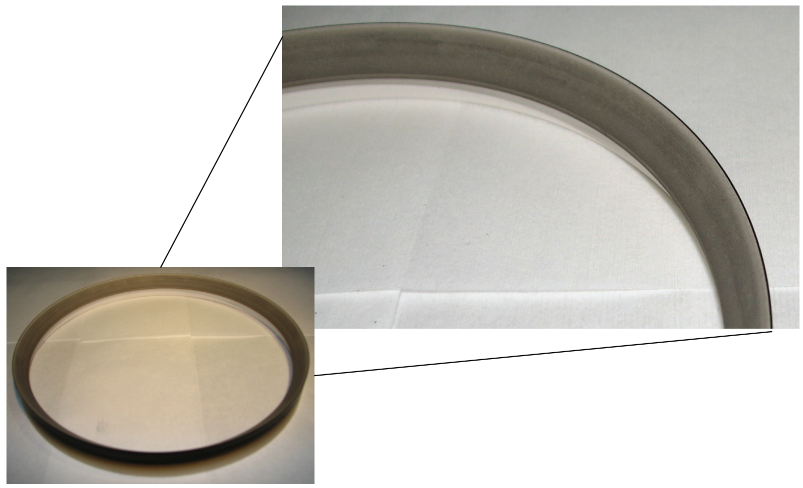

Figure 19 Outer erosion rings from the H6MS after the wear test. As indicated by the measured outer wall grazing line (see Figure 18), the outer wall was very well shielded, resulting in a film of backsputtered carbon that covered the entire outer wall.

The average erosion rate measured by the CMM profilometry is plotted in Figure 20 for various trials of the H6 in the US and MS configurations. Data from the experiments at 300 V in Ref. [3] are shown for comparison. The CMM noise threshold has been estimated to be approximately 1 µm/h. All cases for the H6MS are below this noise threshold. For the 800 V, net deposition was measured, which indicated that magnetic shielding was effective over the course of the wear test.

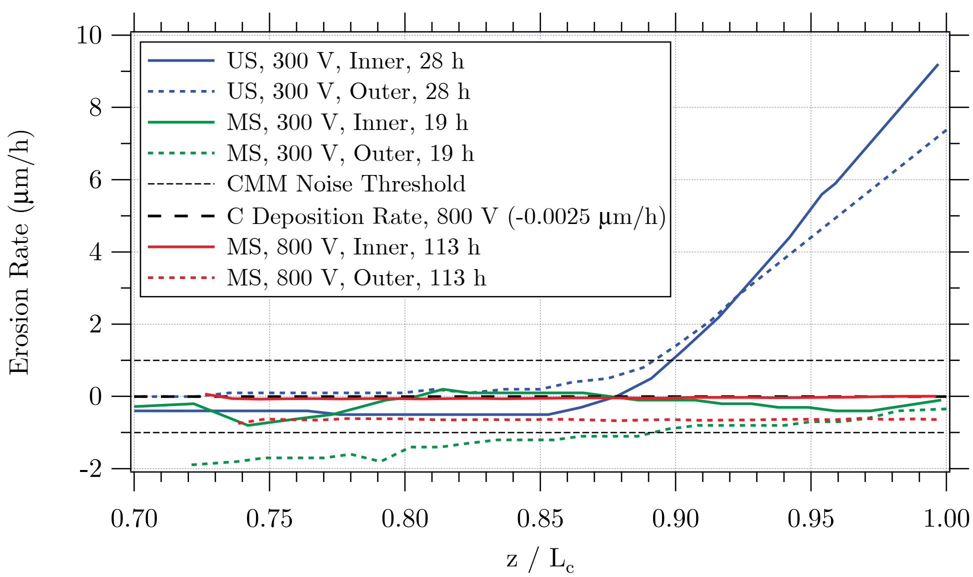

Figure 20 Average erosion rate measured by the CMM for the US and MS configurations of the H6 Hall thruster. Data from the experiments at 300 V in Ref. [3] are shown for comparison. Net deposition was measured at 800 V for the H6MS during the wear test, indicating that magnetic shielding was achieved.

IV. Discussion

Completing the 113 h wear test has advanced the demonstration of magnetic shielding to 50% higher specific impulse (2000 to 3000 s) and 50% higher power density (6 to 9 kW in the same thruster). Highly reliable operation was sustained throughout the wear test as evidenced by every diagnostic used to monitor thruster health. Performance was maintained at 62% efficiency and thrust was constant over a 100 h window. Discharge current oscillations were unchanged in frequency and magnitude over the entire test and the plasma never self-extinguished. Temperatures of the components were maintained at levels consistent with component limitations typical of flight thrusters. Based on these results, it can be generally concluded that the performance, stability, and thermal characteristics of magnetically shielded Hall thrusters at 3000 s specific impulse are compatible with flight applications.

Although the front pole pieces and cathode keeper components were not formally controlled for during the wear test, new insight was gained concerning how these components might wear in magnetically shielded Hall thrusters. The front pole pieces showed evidence of carbon deposition over most of their surfaces, but were relatively clean nearest the discharge chamber walls. These locations correspond to field lines with relatively high electron temperatures and because the poles are at facility ground, the possibility of strong electric fields being directed at the pole piece is likely. These regions though have low plasma densities, which will limit the flux of ions to the poles. We estimate that the sputtering rate in these regions is close to the carbon backsputter rate since the poles were not bare metal after the test and showed no apparent evidence of sputtering. Covering the pole pieces with a sputter resistant coating (e.g., boron nitride, alumina, graphite, or diamond) would likely reduce the sputtering rate to negligible values and eliminate pole piece erosion as a failure mechanism. Similarly, we expect keeper erosion to be mitigated through proper materials selection. The cathode used here already has a graphite keeper and even though a ring discoloration was present, machining marks on the keeper face are still visible. Investigations to be conducted in 2014 will seek to: 1) quantify the erosion rates on these components through physics-based modeling and laboratory experiments and 2) identify engineering solutions to eliminate these possible wear mechanisms as life-limiters of the thruster.

While possibly limiting the performance achieved at 3000 s specific impulse, the asymmetries present in the magnetic field topology proved beneficial in these experiments since they essentially allowed us to execute two independent tests of magnetic shielding physics. The outer wall, being very well shielded by virtue of a grazing field line that extended deep in to the channel, demonstrated clearly that magnetic shielding is achievable at 3000 s specific impulse. The inner wall grazing field line did not extend as deep towards the anode and provided an opportunity to test the predictive capabilities of the physics-based simulations used to compute erosion. We made specific predictions about the locations where higher erosion rates would persist and the wear test showed excellent agreement. The difference in plasma conditions between these two grazing field lines also will inform the design of a new 12.5 kW thruster now being designed by the GRC and JPL team.

Net deposition of carbon was observed to varying degrees on the inner and outer rings. However, observing net deposition does not necessarily establish the upper limit of the erosion rate as the backsputter rate [3]. As illustrated in Figure 21, this is because carbon is being deposited and sputtered by xenon ions that erode the BN wall. Under conditions where there is net deposition of carbon, the erosion rate is reduced and this reduction depends on several factors, most critically, the ratio of sputter yields of the boron nitride (BN) wall material and carbon. The actual erosion rate due to xenon bombardment on BN, that is, the erosion rate that would persist if the carbon backsputter rate (R_c) were zero, is given by [3]

$$\varepsilon_{Xe-BN} \leq \alpha R_C \frac{\rho_C m_{BN}}{\rho_{BN} m_C} \frac{Y_{Xe-BN}}{Y_{Xe-C/BN}} \approx 2 R_C \frac{Y_{Xe-BN}}{Y_{Xe-C/BN}}, \tag{1}$$

if the sticking coefficient (α) is unity. Eqn. (1) establishes an upper bound on the erosion rate that is dependent on the sputtering yield ratio. If the yield ratio is of order unity, the measured carbon backsputter rate may be used to establish a maximum for the BN erosion rate. When the yield ratio is greater than one, the maximum BN erosion rate could be greater than the backsputter rate, but it could also be much less. This is an indeterminate case that could span orders of magnitude in our estimate of the BN erosion rate. Thus, the BN to C/BN yield ratio is a critical parameter in our interpretation of the rings becoming coated with a film.

Interpretation of carbon deposition on the walls is complicated by uncertainty in the sputter yields of carbon and BN under low-energy Xe impact. Our review of the literature [3] places the yield ratio on the order of one to ten in the energy range of 50-200 eV. Using Eqn. (1), this would result in a maximum erosion rate of about 0.05 μm/h (0.0025×2×10). The actual erosion rate could be much lower than this or actually zero if the ion energy is below the sputtering threshold. We estimate that the erosion rate did not significantly exceed 0.025-0.05 um/h anywhere on the wall surfaces, which is a factor of 200-400 lower than the H6US operating at 300 V, 6 kW. Since unshielded Hall thrusters operating at high specific impulse erode at significantly higher rates than the H6US at 2000 s, we estimate that the H6MS operating at 3000 s specific impulse erodes as much as a factor of 1000 lower than unshielded, high specific impulse Hall thrusters (Figure 22).

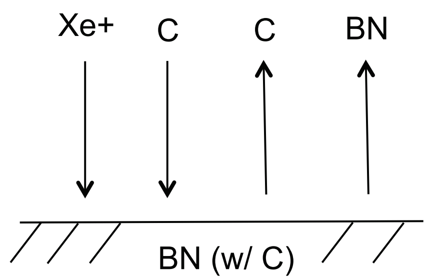

Figure 21 At the surface of the boron nitride (BN) wall, carbon backsputtered from the graphite-lined vacuum chamber wall arrives while high-energy xenon ions sputter both carbon (C) and BN.

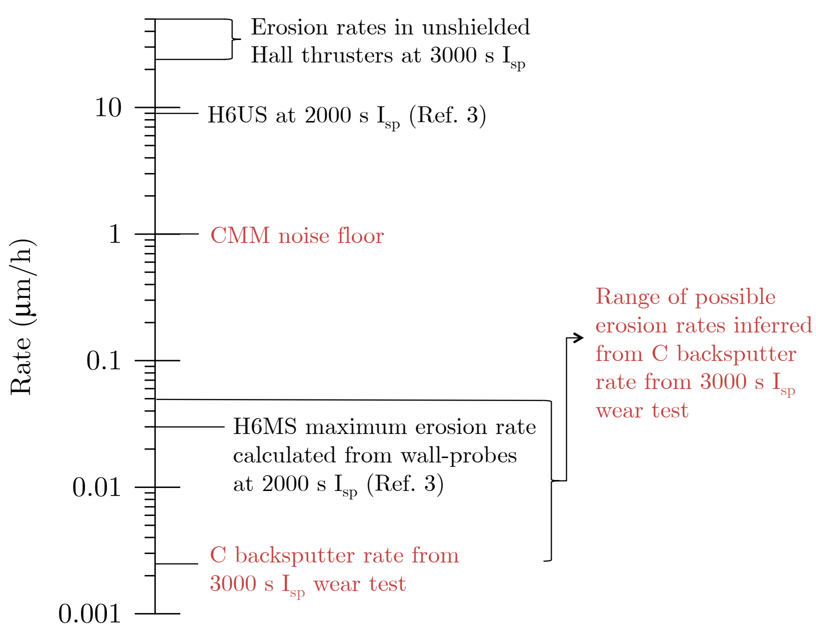

Figure 22 Illustration of the various rates encountered in these experiments (red txt) and other relevant cases. A two to three order of magnitude reduction of wear rate is estimated for the H6MS operating at 3000 s specific impulse relative to unshielded Hall thrusters.

V. Conclusion

Magnetically shielded operation of a 3000 s specific impulse Hall thruster has been demonstrated during a 113 h wear test during which erosion rates were reduced by orders of magnitude relative to unshielded Hall thrusters. The wear test extends the demonstrated capability of magnetic shielding by 50% in terms of specific impulse (2000 to 3000 s) and power density (6 to 9 kW on the same thruster). The success of this experiment is a critical step forward for the propulsion system envisioned for the Asteroid Retrieval Mission (ARM). ARM will require 2.5 times higher propellant throughput per unit power than has been previously demonstrated and this wear test shows that such capability is well within reach of magnetic shielding technology.

The plasma discharge was exceptionally stable throughout the wear test. Thrust, discharge current, and plume profiles were essentially unchanged. A total efficiency of 62% was achieved at 3000 s specific impulse. The wear test revealed new features of magnetically shielded Hall thrusters not previously observed. A ring of discoloration on the graphite keeper appeared, but did not seem to cause significant erosion. Deposition patterns on the pole pieces were non-uniform and suggested that regions nearest the discharge chamber were subject to a higher ion flux perhaps leading to low rates of sputtering. Since neither the cathode or the pole pieces were controlled aspects of this wear test, additional testing is planned to study these potential wear mechanisms in further detail. Materials selection and magnetic circuit design margin are expected to minimize the impact of these potential wear mechanisms on the service life of magnetically shielded Hall thrusters. Magnetic shielding of the discharge chamber walls was demonstrated as evidenced by the appearance of net carbon deposition on the insulator rings and profilometry of the rings after the wear test. Physics-based simulations predicted correctly that the inner wall would exhibit regions where the shielding would be reduced relative to the well-shielded outer wall. These regions of higher relative erosion rates were caused by limitations of the thruster hardware and are not fundamental to Hall thruster design. A new 12.5 kW thruster now being designed by the GRC and JPL team will mitigate this minor limitation with a magnetic circuit capable of providing the necessary field topology at 3000 s specific impulse.

Acknowledgments

The research described in this paper was carried out at the Jet Propulsion Laboratory, California Institute of Technology, under a contract with the National Aeronautics and Space Administration and funded through the Space Technology Mission Directorate's In-Space Propulsion Project (Tim Smith, Program Manager). The authors are indebted to Ray Swindlehurst and Nowell Niblett for their assistance throughput the test campaign constructing and implementing the test apparatus and maintaining the vacuum facility.

References

[1] De Grys, K. H., Mathers, A., Welander, B., and Khayms, V., "Demonstration of 10,400 Hours of Operation on 4.5 kW Qualification Model Hall Thruster," AIAA Paper 2010-6698, July 2010.

[2] Mikellides, I. G., Katz, I., Hofer, R. R., Goebel, D. M., De Grys, K. H., and Mathers, A., "Magnetic Shielding of the Acceleration Channel in a Long-Life Hall Thruster," Physics of Plasmas 18, 033501 (2011).

[3] Hofer, R. R., Goebel, D. M., Mikellides, I. G., and Katz, I., "Design of a Laboratory Hall Thruster with Magnetically Shielded Channel Walls, Phase II: Experiments," AIAA-2012-3788, July 2012.

[4] Mikellides, I. G., Katz, I., and Hofer, R. R., "Design of a Laboratory Hall Thruster with Magnetically Shielded Channel Walls, Phase I: Numerical Simulations," AIAA Paper 2011-5809, July 2011.

[5] Mikellides, I. G., Katz, I., Hofer, R. R., and Goebel, D. M., "Design of a Laboratory Hall Thruster with Magnetically Shielded Channel Walls, Phase III: Comparison of Theory with Experiment," AIAA-2012-3789, July 2012.

[6] Mikellides, I. G., Katz, I., Hofer, R. R., and Goebel, D. M., "Magnetic Shielding of Walls from the Unmagnetized Ion Beam in a Hall Thruster," Applied Physics Letters 102, 2, 023509 (2013).

[7] Mikellides, I. G., Hofer, R. R., Katz, I., and Goebel, D. M., "The Effectiveness of Magnetic Shielding in High-Isp Hall Thrusters," AIAA Paper 2013-3885, July 2013.

[8] Goebel, D. M., Hofer, R. R., Mikellides, I. G., Katz, I., Polk, J. E., and Dotson, B., "Conducting Wall Hall Thrusters," Presented at the 33rd International Electric Propulsion Conference, IEPC-2013-276, Washington, DC, Oct 6-10, 2013.

[9] Kamhawi, H., Huang, W., Haag, T., Soulas, G., Shastry, R., Williams, G., Smith, T., Mikellides, I. G., and Hofer, R. R., "Design and Performance Evaluation of the NASA-300ms 20 kW Hall Effect Thruster," Presented at the 33rd International Electric Propulsion Conference, IEPC-2013-444, Washington, DC, Oct 6-10, 2013.

[10] Conversano, R. W., Goebel, D. M., Hofer, R. R., Matlock, T. S., and Wirz, R. E., "Magnetically Shielded Miniature Hall Thruster: Development and Initial Testing," Presented at the 33rd International Electric Propulsion Conference, IEPC-2013-201, Washington, DC, Oct 6-10, 2013.

[11] Manzella, D. H., Jacobson, D. T., and Jankovsky, R. S., "High Voltage SPT Performance," AIAA Paper 2001-3774, July 2001.

[12] Jacobson, D. T., Jankovsky, R. S., Rawlin, V. K., and Manzella, D. H., "High Voltage TAL Performance," AIAA Paper 2001-3777, July 2001.

[13] Pote, B. and Tedrake, R., "Performance of a High Specific Impulse Hall Thruster," Presented at the 27th International Electric Propulsion Conference, IEPC-2001-35, Pasadena, CA, Oct. 15-19, 2001.

[14] Hofer, R. R. and Gallimore, A. D., "High-Specific Impulse Hall Thrusters, Part 2: Efficiency Analysis," Journal of Propulsion and Power 22, 4, 732-740 (2006).

[15] Hofer, R. R. and Gallimore, A. D., "High-Specific Impulse Hall Thrusters, Part 1: Influence of Current Density and Magnetic Field," Journal of Propulsion and Power 22, 4, 721-731 (2006).

[16] Hofer, R. R., "Development and Characterization of High-Efficiency, High-Specific Impulse Xenon Hall Thrusters," Ph.D. Dissertation, Aerospace Engineering, University of Michigan, Ann Arbor, MI, 2004. (Also NASA/CR-2004-213099)

[17] Kamhawi, H., Manzella, D., Pinero, L., and Haag, T., "In-Space Propulsion High Voltage Hall Accelerator Development Project Overview," Presented at the 57th JANNAF Propulsion Meeting, Colorado Springs, CO, May 3-7, 2010.

[18] Jacobson, D. T. and Manzella, D. H., "Elimination of Lifetime Limiting Mechanism of Hall Thrusters," United States Patent No. 7,500,350 (Mar. 10, 2009).

[19] Brophy, J. R., Gershman, R., Landau, D., Polk, J., Porter, C., Yeomans, D., Allen, C., Williams, W., and Asphaug, E., "Asteroid Return Mission Feasibility Study," AIAA Paper 2011-5565, July 2011.

[20] Brophy, J. and Oleson, S., "Spacecraft Conceptual Design for Returning Entire near-Earth Asteroids," AIAA-2012-4067, July 2012.

[21] Raitses, Y., Staack, D., Keidar, M., and Fisch, N. J., "Electron-Wall Interaction in Hall Thrusters," Physics of Plasmas 12, 057104 (2005).

[22] Raitses, Y., Staack, D., Smirnov, A., and Fisch, N. J., "Space Charge Saturated Sheath Regime and Electron Temperature Saturation in Hall Thrusters," Physics of Plasmas 12, 073507 (2005).

[23] Staack, D., Raitses, Y., and Fisch, N. J., "Temperature Gradient in Hall Thrusters," Applied Physics Letters 84, 16, 3028 (2004).

[24] Linnell, J. A. and Gallimore, A. D., "Internal Plasma Potential Measurements of a Hall Thruster Using Xenon and Krypton Propellant," Physics of Plasma 13, 9, 093502 (2006).

[25] Linnell, J. A. and Gallimore, A. D., "Internal Plasma Potential Measurements of a Hall Thruster Using Plasma Lens Focusing," Physics of Plasmas 13, 103504 (2006).

[26] Haas, J. M., Hofer, R. R., Brown, D. L., Reid, B. M., and Gallimore, A. D., "Design of the H6 Hall Thruster for High Thrust/Power Investigation," Presented at the 54th JANNAF Propulsion Meeting, Denver, CO, May 14-17, 2007.

[27] Hofer, R. R., Goebel, D. M., and Watkins, R. M., "Compact High-Current Rare-Earth Emitter Hollow Cathode for Hall Effect Thrusters," United States Patent No. 8,143,788 (Mar. 27, 2012).

[28] Hofer, R. R., Johnson, L. K., Goebel, D. M., and Wirz, R. E., "Effects of Internally-Mounted Cathodes on Hall Thruster Plume Properties," IEEE Transactions on Plasma Science 36, 5, 2004-2014 (2008).

[29] Reid, B. M., Gallimore, A. D., Hofer, R. R., Li, Y., and Haas, J. M., "Anode Design and Verification for a 6-kW Hall Thruster," JANNAF Journal of Propulsion and Energetics 3, 1, 29-43 (2010).

[30] Randolph, T., Kim, V., Kaufman, H., Kozubsky, K., Zhurin, V., and Day, M., "Facility Effects on Stationary Plasma Thruster Testing," Presented at the 23rd International Electric Propulsion Conference, IEPC Paper 1993-093, Seattle, WA, Sept. 13-16, 1993.

[31] Kahn, J., Zhurin, V., Kozubsky, K., Randolph, T., and Kim, V., "Effect of Background Nitrogen and Oxygen on Insulator Erosion in the SPT-100," Presented at the 23rd International Electric Propulsion Conference, IEPC-93-092, Seattle, WA, Sept. 13-16, 1993.
[32] Hofer, R. R., Goebel, D. M., Snyder, J. S., and Sandler, I., "BPT-4000 Hall Thruster Extended Power Throttling Range Characterization for NASA Science Missions," Presented at the 31st International Electric Propulsion Conference, IEPC-2009-085, Ann Arbor, MI, Sept. 20-24, 2009.
[33] Hofer, R. R., "High-Specific Impulse Operation of the BPT-4000 Hall Thruster for NASA Science Missions," AIAA Paper 2010-6623, July 2010.
[34] Biagioni, L., Kim, V., Nicolini, D., Semenkin, A. V., and Wallace, N. C., "Basic Issues in Electric Propulsion Testing and the Need for International Standards," Presented at the 28th International Electric Propulsion Conference, IEPC Paper 2003-230, Toulouse, France, March 17-21, 2003.
[35] Polk, J. E., Dotson, B., Mikellides, I. G., Hofer, R. R., and Katz, I., "Thermal Characteristics of a Magnetically-Shielded Hall Thruster," Presented at the 33rd International Electric Propulsion Conference, IEPC-2013-440, Washington, DC, Oct 6-10, 2013.
[36] Mikellides, I. G. and Katz, I., "Numerical Simulations of Hall-Effect Plasma Accelerators on a Magnetic-Field-Aligned Mesh," Physical Review E 86, 4, 046703 (2012).
[37] Jorns, B. A. and Hofer, R. R., "Low Frequency Plasma Oscillations in a 6-kW Magnetically Shielded Hall Thruster," AIAA Paper 2013-4119, July 2013.
[38] Mikellides, I. G., Katz, I., Goebel, D. M., Jameson, K. K., and Polk, J. E., "Wear Mechanisms in Electron Sources for Ion Propulsion, 2: Discharge Hollow Cathode," Journal of Propulsion and Power 24, 4, 866 (2008).